Quaternary International 257 (2012) 43–55

Contents lists available at SciVerse ScienceDirect

Quaternary International

journal homepage: www.elsevier.com/locate/quaint

Geochemistry processes of the Djeffara palaeogroundwater (Southeastern Tunisia)

Rim Trabelsi*, Kamel Abid, Kamel Zouari

University of Sfax, National School of Engineers, Laboratory of Radio-Analyses and Environment, Sfax B.P1173 3038, Tunisia

ARTICLE INFO

Article history:
Available online 30 October 2011

ABSTRACT

Environmental stable and radioisotopes have been employed to identify the origin, the recharge mode and geochemical processes controlling groundwater quality. In southeastern Tunisia, where population is growing and water demand for domestic and irrigation activities is increasing, water balance assessment constitutes a serious concern about sustainability of water resources. Isotopic characterization using stable isotopes (δ^2H, $\delta^{18}O$ and $\delta^{13}C$) and radiocarbon (^{14}C) of the Djeffara aquifer system lead to characterization of carbon origin in the system and identification of geochemical processes that control water chemistry. In addition, statistical methods were used to identify the distribution of the salinity. Multivariate statistical analysis (principal component analysis "PCA" and hierarchical cluster analysis "HCA") revealed the main sources of groundwater mineralization. The main reactions responsible for the hydrochemical evolution in the Djeffara groundwater fall into three categories: (1) mixing process; (2) dissolution of salts; and (3) cation exchange process. Djeffara groundwater shows markedly low ^{14}C activities, confirming that the aquifer has limited modern recharge. The modelling of isotopic evolution of the dissolved inorganic carbon (DIC) pool indicates the presence of additional source of carbon ($\delta^{13}C \approx -5‰$) typical for mantle CO_2 which can explain the variability of $\delta^{13}C$ and ^{14}C activities observed in DIC pool of groundwater samples.

© 2011 Elsevier Ltd and INQUA. All rights reserved.

1. Introduction

Over the past decades, the isotopes of carbon and water molecules have been widely applied as natural tracers in hydrological and hydrogeological studies. These tracers are particularly useful tools for groundwater investigation in semiarid and arid regions to identify the flow paths, to assess mixing patterns between different groundwater masses, and to estimate groundwater residence time (Fontes, 1980; Clark and Fritz, 1997; Cook and Herczeg, 2000; Etcheverry, 2002). In this study, isotopic tools are used in combination with statistical analysis methods, particularly principal components analysis (PCA) and hierarchical cluster analysis (HCA).

The PCA is widely used as it is an unbiased method which can indicate associations between samples and/or variables (Wenning and Erickson, 1994). This method is employed to reduce the dimensionality of the data set by explaining the correlation among a large set of variables in terms of a small number of underlying factors, or principal components, without losing much information (Jackson, 1991; Meglen, 1992), and allows assessment of associations between variables, since they indicate participation of individual chemical species.

The hierarchical cluster analysis (HCA) indicates groupings of samples by linking inter-sample similarities and illustrates the overall similarity of variables within the data set (Vega et al., 1998). The application of these statistical methods in combination with geochemical data of Djeffara groundwater allows identification of mixed water and palaeogroundwater components.

In the arid and semi-arid climate in southern Tunisia, groundwater constitutes the main water resources of the region. The Djeffara plain is a coastal area located in southeastern Tunisia, in a relatively populated region. This area is currently undergoing a significant increase in water demand. The structural and geological setting of this plain have produced a multilayered aquifer system which constitutes the main water resource in southeastern Tunisia.

Several hydrogeologic studies have investigated the aquifer system of the Djeffara (Gonfiantini et al., 1974; Mamou, 1990). These studies have shown that major-ion chemistry of Djeffara groundwater could be explained by the reaction of these waters with rocks or sediments through which they flow.

Using environmental isotopes, it has been established that recent recharge of the Djeffara aquifer system is very limited. The

* Corresponding author.
E-mail addresses: rimaenis@yahoo.fr (R. Trabelsi), kamel_hydrology@hotmail.com (K. Abid), kamel.zouari@enis.rnu.tn (K. Zouari).

1040-6182/$ – see front matter © 2011 Elsevier Ltd and INQUA. All rights reserved.
doi:10.1016/j.quaint.2011.10.029

aquifer recharge, particularly in its northern parts (Djeffara of Gabes) can be maintained only through upflow leakage of palaeogroundwater from the Continental Intercalaire aquifer (Trabelsi et al., 2009).

In this study, hydrogeological, hydrochemical and isotopic information from the Djeffara groundwater system will be combined and used to determine the main factors and mechanisms controlling the chemistry, and to model the isotopic evolution of the dissolved inorganic carbon (DIC) in the deep coastal aquifer of the Djeffara plain. The main issues that will be addressed by this study include the use of statistical techniques (PCA and HCA) in classifying water samples according to their hydrochemical parameters; identification of hydrologic and geologic factors in controlling the groundwater chemistry; and the characterization of carbon chemistry in the aquifer system.

2. Study area

The Djeffara basin extends over all the coastal plain from the Skhira region in northern Gabes (southeastern Tunisia) to the Libyan borders. This plain, whose surface is about 15 000 km^2, is

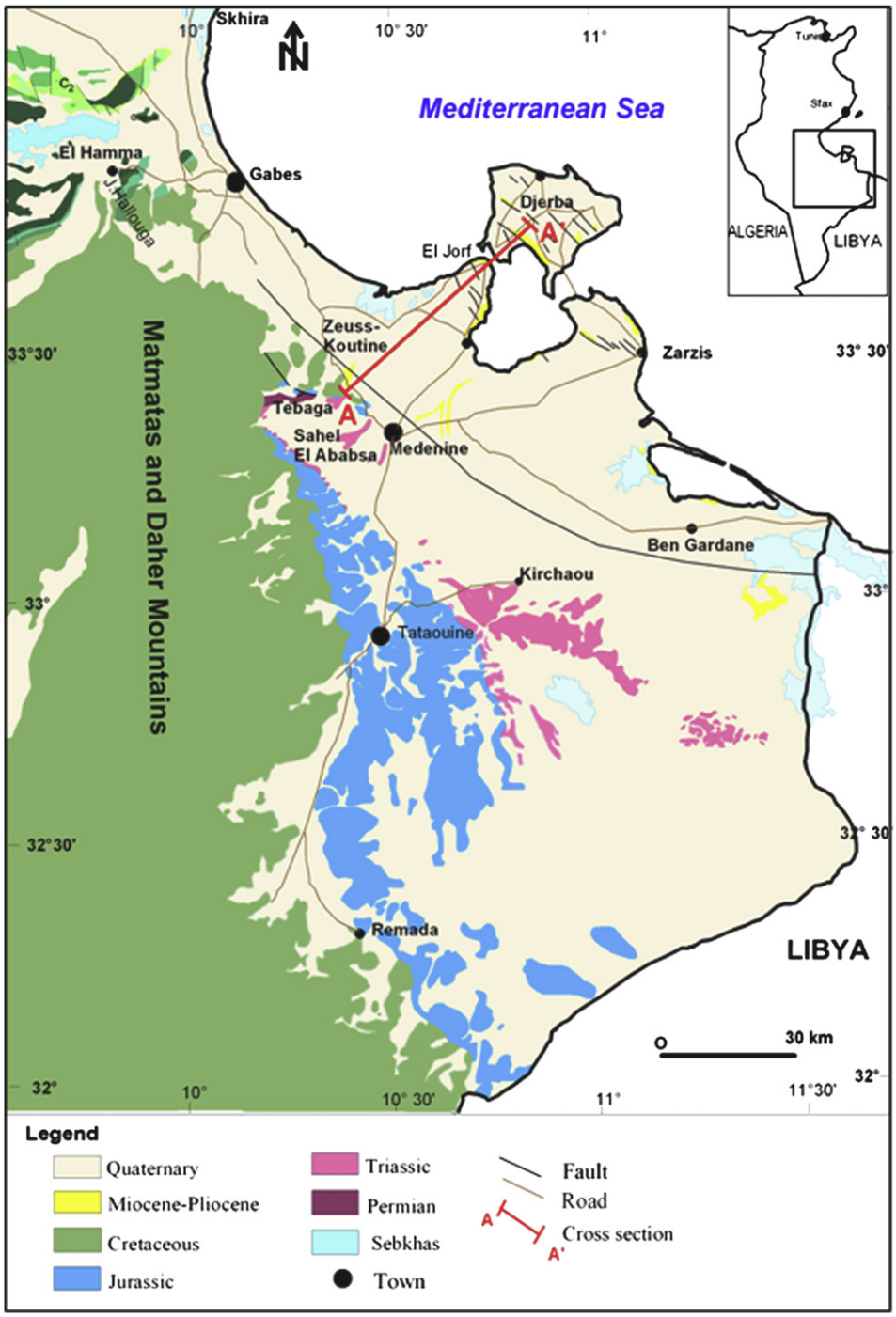

Fig. 1. Geology and location map of Djeffara plain south-eastern Tunisia.

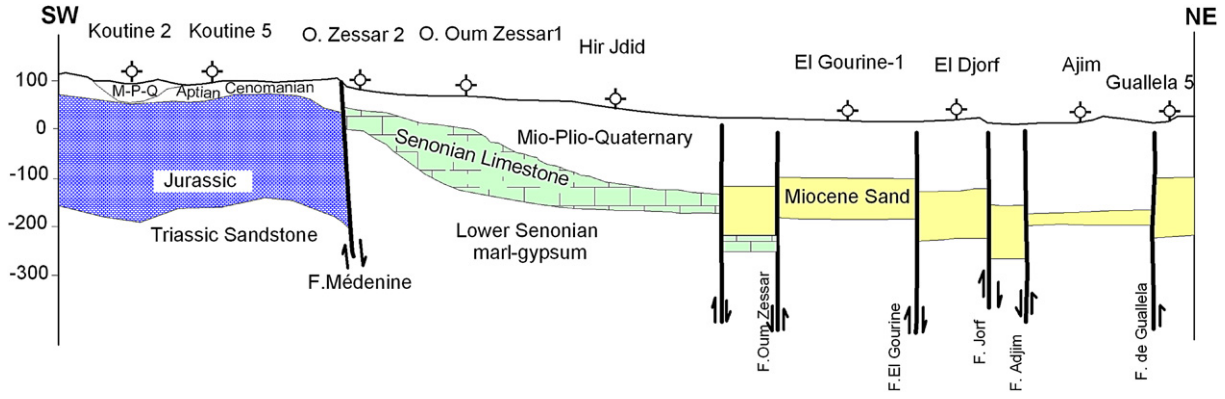

Fig. 2. AA' cross section showing the hydraulic connection between aquifer levels (Ben Baccar, 1982 modified).

limited to the west by the Matmata and Daher mountains and to the east by the Gulf of Gabes and the Mediterranean Sea (Fig. 1).

The climate of the study area is arid to semi-arid, and presents extreme irregularity due to the fact that it is submitted to (i) the dry and hot Saharan air coming from the southwest of the Djeffara basin and to (ii) relatively wet and moderate air from the Gulf of Gabes (Mediterranean Sea) (Kallel, 2003). The mean annual rainfall ranges between 225 to less than 100 mm/year, and it decreases from the north to the south and from the coast towards the west. The mean annual temperature is about 20.6 °C, and the evapotranspiration rate is up to 1700 mm/year.

3. Geology and hydrogeology

The Djeffara plain presents a complete stratigraphic sequence from Late Permian to recent Quaternary with a Permian sequence in the Tebaga of Medenine, the oldest rock exposed in Tunisia (Fig. 1) (Castany, 1954; Bouaziz, 1995). The lithology includes a succession of marine and continental sedimentary deposits whose thickness varies widely from the north to the south and from the east to the west (Bouaziz, 1995; Bouaziz et al., 2002; Gabtni et al., 2009).

The Djeffara basin constitutes a NW–SE trending coastal plain which is strongly affected by tectonic deformations and faults in different directions indicating a complex and polyphase structural history (Bouaziz et al., 2002; Gabtni et al., 2009). The tectonic activities resulted in the production of a large sedimentary basin bounded by deep faults. The Medenine Fault is one of the prominent features that bound the Djeffara aquifer from the southwest (Fig. 1). The basin was downthrown to the NE of the faults, and was filled with thick successions of Neogene (Miocene) to Quaternary sediments (Benton et al., 2000).

All these factors have led to a multilayered aquifer system lodged in carbonate formations of Senonian, Turonian and Jurassic and in detrital formations of Mio-Plio-Quaternary. In the northern part of the Gabes region, the Djeffara aquifer is present in Miocene continental deposits whose thickness increases from 25 to 80 m, towards the sea. Miocene deposits were produced after the post-Cretaceous erosion (Bouaziz, 1995; Benton et al., 2000) and they are red clays with intercalated conglomeratic and sandy layers. The permeability of this aquifer ranges from 2×10^{-5} to 4×10^{-4} m/s. In the southern part of Gabes, the Djeffara aquifer consists of Senonian limestones which are strongly fissured. The bottom of this aquifer is formed by 50 m of Lower Senonian marl and gypsum. The thickness of these limestones is variable, up to 500 m, and the transmissivity ranges from 0.9×10^{-3} to 345×10^{-3} m^2/s. The western part, in Matmatas, El Hamma and Chenchou regions, the Djeffara aquifer is present in the Turonian dolomites and fissured limestones. These carbonate formations are characterized by high transmissivity, exceptionally reaching 1200×10^{-3} m^2/s in the Chenchou area, where the tectonic deformation is particularly intense.

In the Zeuss koutine region, the aquifer consists of Jurassic fissured limestone and dolomite. This aquifer is covered by marly limestone and impermeable marls. The exploitation depth increases towards the southeast and north.

In the southern part of the basin, in the Medenine region, the Miocene sandstone constitutes the principal water-bearing formation. It is confined over all the Medenine coastal plain, where it is covered by a hundred meters of Mio-Pliocene marls and clays (Fig. 2). Although there are large changes of lithology and thickness of water-bearing horizons, all aquifer levels of the Djeffara plain are hydraulically connected through the existing faults (Fig. 2).

Hydraulic continuity between the Djeffara aquifer formations is confirmed by the piezometric map showing concordant hydrodynamic levels (Fig. 3). The Djeffara aquifer shows a general SW–NE flow, from El Hamma, Matmata relief and Medenine fault towards the Mediterranean Sea, in accordance with the structure. The recharge of this aquifer is ensured from three main origins:

(i) The upflow leakage from the Continental Intercalaire (CI) aquifer through El Hamma fault in Gabes region (Trabelsi et al., 2009)

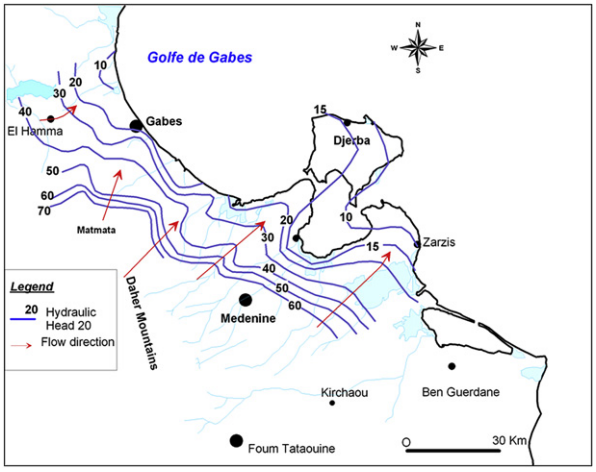

Fig. 3. Piezometric map of the Djeffara aquifer system (Trabelsi, 2009).

Table 1
Isotopic and geochemical data for the studied aquifers.

WellN°	Aquifer names	Total depth	EC	*T*	pH	Na^+	Ca^{2+}	Mg^{2+}	K^+	Cl^-	SO_4^{2-}	HCO_3^-	TDS	$\delta^{18}O$	δ^2H	$\delta^{13}C$	^{14}C
		(m)	(μS/cm)	(°C)		(mg/l)								(‰ VSMOW)		(‰ VPDB)	(pmc)
1	Jurassic (Zeuss koutine)	100	2600	29.2	8.1	242.7	196.1	57.1	0.0	308.2	609.6	189.1	1729	−5.93	−33.2		
2	Jurassic (Zeuss koutine)	161	5230	26.9	8.3	627.7	409.4	110.8	36.3	1156.0	785.4	213.5	3570	−6.07	−37.8	−5.9	20.2
3	Jurassic (Zeuss koutine)	243	3420	28.1	7.5	467.4	196.7	84.1	197.4	627.4	935.4	176.9	2510	−5.75	−34.4	−7.2	26.0
4	Jurassic (Zeuss koutine)	577	6120	27.6	7.7	790.9	452.7	114.9	26.0	1609.1	937.0	207.4	4225	−6.17	−39.7	−5.9	13.8
5	Turonian	550	4060	31	7.5	397.1	388.2	87.4	16.0	547.1	1131.3	134.2	3134	−7.34	−52.2	−5.5	11.0
6	Turonian	140	3900	27	7.6	357.7	301.7	85.2	10.7	484.2	1023.6	36.6	2622	−6.55	−46.2		
7	Turonian	354	3480	23.3	7.2	370.0	274.5	102.6	0.0	500.2	1129.3	115.9	2640	−6.97	−49.3	−6.2	12.5
8	Turonian	300	2700	26.1	7.6	313.8	203.8	58.2	0.0	368.5	803.6	262.3	1930	−4.33	−30.4	−7.2	12.5
9	Turonian	70	9650	20	8.0	884.7	842.6	353.0	89.5	1995.7	2455.1	152.5	8029	−6.03	−36.6		
10	Turonian	544	3720	25.7	7.4	451.8	369.0	99.2	27.3	618.6	1228.7	91.5	2940	−7.22	−54.2		22.7
11	Turonian	67	3450	23.7	7.2	268.1	382.6	119.6	0.0	376.6	1386.1	176.9	2820	−6.05	−32.5	−7.8	43.0
12	Turonian	67	3080	24.5	7.0	281.3	383.1	95.4	31.8	337.7	1120.1	226.0	2600	−5.96	−34.5	−6.6	37.0
13	Turonian	150	2610	22.7	7.2	243.1	257.2	110.1	0.0	400.5	891.5	183.0	2040	−5.80	−31.9		
14	Turonian	571	3740	25	7.5	394.3	302.9	111.1	0.0	567.2	1263.0	122.0	2870	−7.01	−51.6	−6.5	9.5
15	Turonian	571	3770	24	7.5	367.8	353.0	89.8	20.3	464.8	1244.8	232.0	2960	−7.09	−52.9	−4.7	7.7
16	Turonian	432	4690	20.2	7.5	550.4	382.6	157.8	0.0	939.9	1402.2	122.0	3750	−6.92	−49.7	−5.2	11.4
17	Turonian		3750	24.8	7.5	408.3	300.5	105.1	0.0	584.3	1154.2	122.0	2890	−7.34	−52.2		
18	Senonian		4000	27	8.2	358.0	287.0	84.7	11.5	443.4	1023.6	128.1	2631	−7.01	−48.3		
19	Senonian		3880	35.5	8.1	418.5	266.6	87.0	16.2	531.1	1026.5	164.7	2895	−6.91	−49.9	−9.7	
20	Senonian	66	4250	41.6	7.7	459.2	420.6	68.2	51.5	731.6	1104.7	116.0	3170	−6.90	−54.5	−7.8	8.8
21	Senonian	88	4720	26.7	7.0	512.6	339.1	68.2	53.7	759.5	1258.2	110.0	3530	−7.20	−55.0	−7.4	13.5
22	Senonian	49.5	7170	32.5	7.5	834.2	686.6	102.3	57.2	1443.8	1455.0	170.8	5914	−8.20	−57.4		
23	Senonian	264	4320	30.5	7.5	449.4	403.1	59.4	37.0	748.5	1039.4	140.3	3152	−8.31	−58.6		
24	Senonian	105	7280	29.1	7.8	499.3	302.0	59.8	50.1	666.7	1137.7	122.0	3270	−7.77	−57.1	−7.9	18.5
25	Senonian	90	5180	34	7.7	747.6	432.9	111.0	0.0	940.0	1789.2	61.0	4070	−7.75	−62.7		
26	Senonian		4800	38.0	7.7	680.2	342.0	120.4	0.0	777.2	1512.0	91.5	3560	−7.84	−61.7		
27	Senonian	68	4700	41.0	7.9	511.0	405.5	105.2	0.0	814.0	1316.0	61.0	3360	−7.17	−60.7		
28	Senonian		4660	40.2	7.7	433.1	558.9	100.7	0.0	806.6	1542.4	67.1	3640	−8.18	−65.9		
29	Senonian		4860	42.2	7.8	651.3	448.7	89.9	0.0	857.2	1516.0	103.7	3770	−8.23	−62.9		
30	Senonian	152	4830	40.2	7.8	519.1	451.9	103.2	0.0	788.0	1608.0	54.9	3520	−8.28	−63.4		
31	Senonian		4600	44.0	7.4	316.0	360.2	58.9	0.0	706.8	857.3	85.4	2500	−8.25	−61.1		
32	Senonian		4460	45.6	7.7	566.5	507.3	66.7	0.0	1084.0	1139.2	61.0	3350	−8.29	−62.7		
33	Senonian		4180	46.2	7.5	479.4	416.0	86.1	0.0	797.6	1318.4	79.3	3200	−8.29	−61.1		
34	Senonian	154	3100	31.9	7.3	408.9	345.8	88.0	19.6	565.6	1133.8	134.0	2990	−7.27	−53.8	−6.9	23.5
35	Senonian	199	3820	31.5	8.0	408.6	412.4	85.0	24.3	467.9	1220.4	134.0	3010	−7.01	−51.0	−5.2	12.5
36	Senonian	146	3550	31.9	8.0	356.2	371.9	86.0	10.9	439.9	1118.1	146.0	2770	−7.04	−49.0	−6.0	16.7
37	Senonian	100	3780	27.6	7.9	416.1	240.6	75.5	23.8	517.3	1062.7	146.0	2840	−7.29	−53.0	−6.9	12.3
38	Senonian	130	4100	30	6.9	394.2	367.4	86.8	16.9	650.2	981.9	94.6	3100	−7.42	−52.8		
39	Senonian	250	4200	31	7.6	446.0	433.6	75.8	31.5	708.9	1050.9	134.2	3456	−7.00	−55.3	−7.4	15.8
40	Senonian	85	2580	28	7.6	424.0	507.0	105.0	24.0	632.0	1318.0	134.0	3250	−6.65	−44.8		
41	Senonian	50	3100	22.3	7.8	295.3	275.2	69.2	0.0	452.0	737.6	122.0	2328	−5.94	−35.7	−6.6	32.4
42	Senonian	1500	3500	30	8.1	381.0	118.7	24.9	16.5	508.7	439.2	18.3	2041	−6.80	−50.7		
43	Senonian	1500	3050	25.4	8.8	549.8	87.8	27.7	0.0	673.1	496.4	42.7	1830	−6.78	−50.1		
44	Senonian	200	3500	27	8.0	357.2	355.7	105.2	0.0	513.6	1126.6	109.8	2978	−6.83	−50.5		
45	Senonian	300	3770	22	8.0	404.7	378.9	148.1	23.7	497.9	1266.8	183.0	3326	−5.82	−33.6		
46	Senonian	188	3430	26.8	8.4	351.3	212.0	76.7	26.7	451.3	940.7	140.3	2605	−6.92	−48.9		
47	Senonian	618	3380	27.1	8.0	326.6	291.2	80.8	0.0	440.1	880.1	134.2	3998	−6.95	−48.0		
48	Senonian	0	3400	25.5	6.5	375.0	322.0	91.0	15.0	440.0	1085.0	122.0	3050	−6.98	−48.1		
49	Senonian	275	3450	26.1	7.6	371.0	321.0	94.0	14.0	454.0	1101.0	122.0	2590	−6.97	−47.7		
50	Senonian	225	3400	24.9	7.0	344.0	314.0	84.0	31.0	426.0	993.0	153.0	2700	−6.94	−46.8		
51	Senonian	262	3390	25.9	6.9	342.0	286.0	62.0	22.0	453.0	1015.0	128.0	2700	−6.95	−48.0		

52	Senonian	220	4380	26.5	7.1	461.0	405.0	105.0	23.0	494.0	1470.0	122.0	3840	−6.82	−51.6		
53	Senonian	220	13 000	23	7.5	1100.0	1040.0	930.0	110.0	3199.7	3475.0	292.8	10 370	−6.21	−43.7		9.5
54	Senonian	78.5	3670	26.5	7.3	398.5	359.0	95.8	36.8	599.2	1042.1	140.0	2770	−6.88	−50.4	−5.6	31.0
55	Senonian	575	3330	26.7	6.6	343.0	283.0	83.1	20.2	405.1	983.1	140.0	2650	−6.89	−47.5	−5.6	2.0
56	Senonian	611	3370	27.6	6.7	356.2	295.0	83.2	21.1	414.0	1014.8	140.0	2620	−6.90	−47.9	−6.2	9.2
57	Miocene (Gabes)		7740	24.6	8.1	584.0	482.9	115.6	18.3	923.8	1331.0	134.2	4241	−7.36	−51.7		
58	Miocene (Gabes)		8350	22.8	8.3	1032.9	620.1	160.1	38.7	1706.9	1670.5	152.5	6834	−6.79	−44.1		
59	Miocene (Gabes)		8410	24	7.6	1104.0	624.0	201.0	40.0	2059.0	1944.0	195.0	6430	−7.76	−59.9	−9.7	25.8
60	Miocene (Gabes)		5440	24.3	7.7	455.0	400.0	172.0	16.0	994.0	1344.0	189.0	3750	−7.36	−54.5		
61	Miocene (Gabes)		8090	24.7	7.9	1805.0	656.0	326.0	63.0	2982.0	2856.0	225.0	9340	−6.38	−46.7		
62	Miocene (Gabes)		6210	23.3	7.7	667.0	448.0	163.0	31.0	1278.0	1334.0	170.0	4340	−7.69	−56.7		
63	Miocene (Gabes)		5430	24.1	7.9	575.0	384.0	153.0	24.0	1136.0	1363.0	189.0	3960	−7.51	−53.7	−7.9	10.5
64	Miocene (Gabes)		4860	25.3	7.7	552.0	480.0	115.0	44.0	1136.0	1248.0	195.0	3930	−7.87	−58.8		
65	Miocene (Gabes)	90	4250	22.0	7.9	458.8	392.3	75.1	31.1	663.4	1119.0	128.0	3210	−7.84	−58.8	−6.9	16.2
66	Miocene (Gabes)	65	4720	25.5	6.0	465.1	388.8	82.2	30.1	875.9	1032.5	119.0	3500	−7.91	−57.0		
67	Miocene (Gabes)	143	4170	26.2	6.8	422.6	364.8	86.8	26.2	720.3	1022.6	95.4	3190	−7.56	−55.0		
68	Miocene (Gabes)	80	5140	27.0	6.9	533.1	430.8	90.2	34.4	953.3	1135.0	94.6	3800	−7.80	−58.2		
69	Miocene (Gabes)	140	4210	31.0	8.0	416.9	435.0	90.1	27.1	692.0	1315.5	140.3	3123.0	−7.24	−51.4		
70	Miocene (Gabes)	82	5450	24.0	7.5	570.3	444.4	86.9	28.4	945.0	1129.7	134.2	3205	−7.84	−58.7		
71	Miocene (Gabes)	100	4200	23.0	8.2	436.3	422.3	90.9	26.5	631.8	1238.1	122.0	3337	−7.30	−51.4		
72	Miocene (Gabes)	80	4220	23.7	7.9	421.0	356.2	95.0	12.7	557.8	1139.7	134.2	3206	−7.23	−48.6		
73	Miocene (Gabes)	100	5450	23.2	8.1	650.3	404.4	81.7	28.4	971.3	1236.6	134.2	3964	−7.83	−55.3		
74	Miocene (Gabes)	80	4150	23.9	7.9	445.4	395.9	96.5	28.2	598.0	1169.3	115.9	3206	−7.47	−51.5		
75	Miocene (Gabes)	170	7740	24.6	8.2	958.0	534.4	156.4	0.0	1579.7	1542.3	140.3	5712	−6.63	−45.0		
76	Miocene (Gabes)	95	4090	27.0	8.0	413.0	356.0	86.0	31.0	543.0	1052.0	134.0	2650	−7.39	−51.1		
77	Miocene (Medenine)	300	7790	25.8	8.0	1083.6	618.8	173.8	0.0	1814.9	1844.3	164.7	5750	−4.47	−39.0	−8.2	5.5
78	Miocene (Medenine)	400	5670	25.8	8.0	804.5	413.1	174.2	0.0	984.4	1654.9	146.6	4000	−4.56	−38.2	−7.9	16.0
79	Miocene (Medenine)	300	7110	29.0	8.1	1135.6	381.1	114.0	0.0	1413.9	1920.4	97.6	5150	−5.42	−42.5		
80	Miocene (Medenine)	300	7310	29.8	7.6	1205.6	465.2	111.8	0.0	1435.4	1972.7	97.6	5300	−5.06	−43.0	−8.3	10.3
81	Miocene (Medenine)	290	9640	33.4	7.4	1403.2	303.7	125.4	114.8	2246.0	1425.4	201.3	5810	−6.42	−45.0	−13.5	2.0
82	Miocene (Medenine)	322	8380	31.8	7.7	1158.4	297.7	127.0	341.0	1738.3	1814.7	152.5	5450	−6.30	−48.0	−9.2	4.4
83	Miocene (Medenine)		11 800	33.7	7.5	1781.2	455.3	132.1	0.0	2860.2	1627.2	146.4	7845	−6.11	−41.6	−8.7	2.5
84	Miocene (Medenine)		9090	28.3	7.5	1201.6	356.4	134.4	29.8	1652.9	1893.3	213.5	6257	−6.42	−45.1	−8.2	3.7
85	Miocene (Medenine)	80	3120	25.1	7.5	327.7	202.0	88.1	21.8	410.6	727.7	146.4	2270	−5.74	−38.1		
86	Miocene (Medenine)	80	5000	25.3	7.9	444.9	521.4	199.0	0.0	484.7	2365.1	122.0	4400	−5.93	−37.5		
87	Miocene (Medenine)	90	7220	25.5	7.7	845.7	814.7	133.4	27.6	1302.0	2223.1	134.2	5850	−5.99	−39.2	−6.8	29.5
88	Miocene (Medenine)	87	3750	14.3	8.0	456.5	594.4	134.0	35.9	427.1	2335.6	115.9	4347	−6.00	−38.3	−5.0	
89	Miocene (Medenine)	203	12 750	15.0	7.5	1750.3	817.8	282.2	106.5	2855.4	2947.6	219.6	8925	−6.37	−47.4	−6.9	3.4
90	Miocene (Medenine)	85	3120	14.9	7.7	447.9	281.5	76.7	51.4	495.8	1017.8	146.4	2870	−6.97	−49.1		
91	Miocene (Medenine)	130	5850	25.7	7.5	540.5	767.8	192.0	0.0	937.8	2239.1	158.6	4730	−6.48	−43.2	−7.2	

(ii) The infiltration of rain water through Turonian outcrops in Matmata reliefs (Trabelsi et al., 2009)
(iii) The lateral leakage from Triassic aquifer through the Medenine fault system in the southern part of the basin (Zouari et al., 2010).

4. Materials and methods

4.1. Sampling and analysis

Hydrogeological information was gathered from a sampling network collected from April 2003 until May 2006. Ninety-one groundwater samples from the Miocene, Senonian, Turonian and Jurassic aquifers (Table 1; Fig. 1) were collected during this period. The temperature, pH, and electrical conductivity (EC) were measured in the field. Chemical analyses of Na^+, Ca^{2+}, Mg^{2+}, K^+, HCO_3^-, Cl^-, SO_4^{2-} and NO_3^- were carried out in the Laboratory of Radio-Analyses and Environment (LRAE) of the National Engineering School of Sfax (ENIS: Tunisia), using standard analytical procedures. Major cations (Ca^{2+}, Mg^{2+}, Na^+ and K^+) and anions (Cl^-, SO_4^{2-} and NO_3^-) concentrations were conducted by liquid ion chromatography (HPLC). The total alkalinity (as HCO_3) was determined by titration with 0.01 or 0.1 HCl against methyl orange and bromcresol green indicators.

Stable isotope composition of water samples ($\delta^{18}O$, δ^2H) was determined at the Isotope Hydrology Laboratory of the International Atomic Energy Agency in Vienna (IAEA), using CO_2 equilibration technique for $\delta^{18}O$ (Epstein and Mayeda, 1953) and isotopic exchange with H_2 gas for δ^2H (Colpen et al., 1991), followed by mass-spectrometry measurement. The results are expressed as relative deviations δ (in per mil) from the Vienna standard mean ocean water (VSMOW). The analytical precision of stable isotope analyses (one sigma) was in the order of 0.1‰ for $\delta^{18}O$ and 1‰ for δ^2H.

The tritium content was measured at the IAEA Laboratory using electrolytic enrichment and liquid scintillation spectrometry (Taylor, 1977). The results are expressed in Tritium Units (TU) (one TU is equivalent to one ^3H atom per 10^{-18} atoms of hydrogen) (Clark and Fritz, 1997) with the analytical uncertainty in the order of 0.3 TU.

A total of 38 samples for radiocarbon analyses were collected in the field by precipitating $BaCO_3$. Radiocarbon content in the total dissolved inorganic carbon pool (TDIC) was measured at the LRAE Laboratory through benzene synthesis and liquid scintillation counting (Fontes, 1971). The measured ^{14}C concentrations are expressed as percent modern carbon (pmc) by comparing carbon-14 activities with the radioactivity of the modern radiocarbon standard of Oxalic Acid I ($C_2H_2O_4$) (Taylor, 1987). The results of chemical and isotope analyses of the investigated groundwater samples are presented in Table 1.

4.2. Statistical analysis

In order to identify the most important factors controlling the groundwater geochemistry, a principal component analysis (PCA) was performed using the program STATISTICA 8.0 (StatSoft Inc., 1995). Ten hydrochemical variables (including EC, Na^+, Ca^{2+}, Mg^{2+}, K^+, HCO_3^-, Cl^-, SO_4^{2-}, pH and temperature), and 91 samples were treated using multivariate statistical techniques. The values of the different variables (Table 1) were standardized prior to the multivariate analyses.

Table 2 presents the matrix of correlation coefficients for the hydrochemical data in Djeffara aquifer system. The correlation coefficient matrix measures how well the variance of each parameter can be explained by relationships with other constituents. Diagonalization of the correlation matrix transforms the original p correlated variables into p uncorrelated (orthogonal) variables called principal components (PCs), which are weighted linear combinations of the original variables (Mellinger, 1987; Meglen, 1992; Wenning and Erickson, 1994). The characteristic roots (eigenvalues) of the PCs are a measure of their associated variances, and the sum of eigenvalues coincides with the total number of variables. Correlation of PCs and original variables is given by loadings, and individual transformed observations are called scores. Eigenvalues and eigenvectors were calculated for the covariance matrix. Then, the data were transformed into factors. Table 3 presents the eigenvalues and the cumulative percentages of variance associated with each factor. Factor score coefficients are derived from the factor loadings. Factor scores are computed for each sample by a matrix multiplication of the factor score coefficient with the standardized data. The value of each factor score (Table 4) represents the importance of a given factor at the sample site. A factor score $>+1$ indicates intense influence by the process. Very negative values (<-1) reflect areas virtually unaffected by the process, and near-zero scores reflect areas with only a moderate effect of the process. The spatial distribution of the factors (and hence the hydrochemical process represented by them) can be assessed by a classed map of the factor scores representing each factor.

In the hierarchical cluster analysis (HCA) method, the distance between samples is used as a measure of similarity (Vega et al., 1998). Among the hierarchical agglomerative cluster analysis techniques, such as the complete linkage (furthest neighbor), average linkage (between and within groups) and Ward's method, the last one was selected for this study. Ward's method clustering algorithm, using squared Euclidean distances as a measure of similarity/diversity metric, has been proven to be an extremely

Table 2
Correlation matrix of 10 variables computed from chemical data of the current sampling. Bold values indicate a significant correlation factor.

	K	pH	T °C	EC	Ca	Mg	Na	HCO_3	Cl	SO_4
K	**1**									
pH	−0.06	**1**								
T °C	−0.10	−0.003	**1**							
EC	0.34	0.091	−0.16	**1**						
Ca	0.12	0.050	−0.11	0.80	**1**					
Mg	0.26	0.033	−0.24	0.74	0.70	**1**				
Na	0.34	0.131	−0.04	**0.88**	0.53	0.46	**1**			
HCO_3	0.31	−0.046	−0.41	0.40	0.29	0.48	0.30	**1**		
Cl	0.37	0.092	−0.06	**0.94**	0.67	0.66	**0.94**	0.40	**1**	
SO_4	0.26	0.074	−0.17	**0.87**	**0.84**	0.76	0.69	0.30	0.72	**1**

Table 3
Loading of the components obtained from principal component analysis, with two factors: Eigenvalue derived by factor analysis, and cumulative % explained by factors.

Variables	Component 1	Component 2	Component 3
EC	0.93	0.17	−0.10
pH	0.09	0.40	0.65
T °C	−0.20	0.75	−0.36
Ca	0.81	0.04	0.22
Mg	0.80	−0.17	0.17
Na	0.86	0.22	−0.15
K	0.41	−0.18	−0.58
A	0.28	−0.80	0.01
Cl	0.93	0.17	−0.13
SO_4	0.89	0.01	0.15
Eigenvalues	4.86	1.54	1.04
Cumulative %	48.65	64.01	74.38

Table 4
Factor Scores of chemical data (in meq/L) of the current groundwater samples.

N°	Component 1	Component 2	Component 3	N°	Component 1	Component 2	Component 3
1	−2.6	−0.5	0.8	47	−1.3	−0.3	0.9
2	0.1	−1.0	0.8	48	−1.1	−2.5	−1.3
3	−0.9	−1.1	−2.5	49	−1.3	−0.6	0.3
4	0.8	−0.8	−0.2	50	−1.5	−1.3	−0.8
5	−1.2	0.6	−0.2	51	−1.6	−1.5	−0.9
6	−1.6	−0.1	0.2	52	−0.4	−0.8	−0.5
7	−1.6	−0.2	0.0	53	10.6	−1.5	0.5
8	−2.1	−1.6	0.4	54	−1.1	−0.7	−0.5
9	5.3	0.2	0.8	55	−1.7	−1.2	−1.4
10	−0.8	−0.3	−0.2	56	−1.6	−1.3	−1.3
11	−1.0	−1.5	0.2	57	0.3	0.4	1.0
12	−1.1	−2.2	−0.6	58	2.9	1.0	1.1
13	−2.0	−1.2	0.1	59	3.5	0.2	0.1
14	−1.2	−0.1	0.4	60	0.1	−0.4	0.6
15	−0.8	−2.1	0.3	61	7.1	0.7	−0.1
16	0.0	−0.4	0.6	62	0.8	−0.1	0.4
17	−1.3	−0.1	0.4	63	0.4	−0.5	0.7
18	−1.5	−0.1	1.1	64	0.4	−0.3	0.0
19	−1.4	0.5	0.2	65	−0.7	−0.4	0.7
20	−0.9	1.5	−1.1	66	−0.7	−1.8	−2.4
21	−0.6	−0.7	−1.3	67	−0.9	−1.4	−1.1
22	2.0	0.6	−0.8	68	−0.2	−0.9	−1.2
23	−1.0	0.5	−0.5	69	−0.6	0.7	0.4
24	−1.0	0.5	−0.2	70	−0.4	0.1	0.0
25	0.3	1.7	0.0	71	−0.5	−0.3	1.2
26	−0.4	1.4	−0.3	72	−0.9	−0.3	0.9
27	−0.9	2.9	−0.2	73	0.1	−0.3	0.9
28	−0.4	2.7	−0.1	74	−0.7	−0.1	0.8
29	−0.3	2.6	−0.4	75	2.0	0.7	1.3
30	−0.4	2.3	−0.2	76	−1.1	−0.3	0.6
31	−2.1	2.4	−1.1	77	2.9	0.2	1.1
32	−0.8	3.4	−0.9	78	1.0	−0.9	1.1
33	−1.1	2.9	−1.1	79	1.6	1.2	0.6
34	−1.2	0.0	−0.6	80	1.9	1.0	−0.1
35	−0.9	0.2	0.4	81	2.5	0.7	−2.6
36	−1.3	0.4	0.6	82	3.0	−0.3	−4.5
37	−1.5	0.1	0.3	83	3.8	2.3	−1.2
38	−1.3	−0.2	−1.2	84	2.3	0.2	−0.7
39	−0.8	0.8	−0.3	85	−2.0	−1.2	−0.1
40	−0.3	−0.4	0.2	86	1.1	−0.5	1.5
41	−2.0	−0.5	0.9	87	2.9	0.4	0.7
42	−3.1	2.1	0.2	88	1.3	−1.1	2.0
43	−2.8	2.1	1.7	89	7.6	−1.5	−0.3
44	−1.2	0.3	1.0	90	−1.2	−1.1	0.5
45	−0.3	−1.4	1.1	91	2.0	−0.3	1.0
46	−1.7	−0.2	1.1				

powerful grouping mechanism (Willet, 1987). Variables used to classify all samples considered in this second analysis and to more identify mixed water components and fossil groundwater were physical parameters (pH, temperature and alkalinity), and stable isotopes contents ($\delta^{18}O$ and $\delta^{2}H$).

5. Results and discussion

5.1. Hydrochemistry

Results of the current sampling are shown in Table 1. The temperature ranges from 14.3 to 46.2 °C (Fig. 4a). There is not a good correlation between temperature and well depth (Trabelsi, 2009), which indicates that the water is derived from the main horizon of the aquifer with rapid leakage from overlying formations. The reported pH values measured at well heads are generally between 6 and 8.8. With the exception of four points (wells No. 42, 55, 48 and 66 with pH of 8.8, 6.6, 6.5 and 6.0, respectively), the waters are relatively well buffered with neutral pH, with a median value of 7.63 (Fig. 4b).

Electrical conductivity (EC) varies between 2580 and 13 000 μS/cm, with an average of 5033 μS/cm; 67% of the samples gave values between 2580 and 5000 μS/cm, and 33% were between 5000 and 13 000 μS/cm (Fig. 4c). This high salinity is determined by the predominance of the major ions SO_4^{2-}, Cl^- and Na^+ (Table 2), which correlate well with the electrical conductivity (Fig. 5). Consequently, the waters are mostly classified as Na–Cl facies, borne out by the fact that the Na–Cl waters are mainly situated downstream, close to the sabkhas and upstream from the Mediterranean Sea. Other water types in the eastern and western zones of the plain present a net enrichment in SO_4^{2-} and Ca^{2+} (Fig. 6).

5.2. Principal component analysis

The results of the PCA are presented in Table 3. The two principal axes of PCA explain 64% of the sampling variance (Fig. 7a). This percentage is relatively low, indicating a limited structuring of the variance, because the chemistry of the water is conditioned by various factors. Axis I (48.65%) is the content factor, which has a highly positive loadings for the variables EC, Cl^-, Na^+, Ca^{2+}, Mg^{2+}, SO_4^{2-} and Cl^-, positive loadings for pH and alkalinity and negative loading for temperature (Fig. 7b).

The hydrochemical items are the dominant solutes in saline water, especially Cl^- and Na^+ ($r = 0.87$ for raw data in Table 3), and

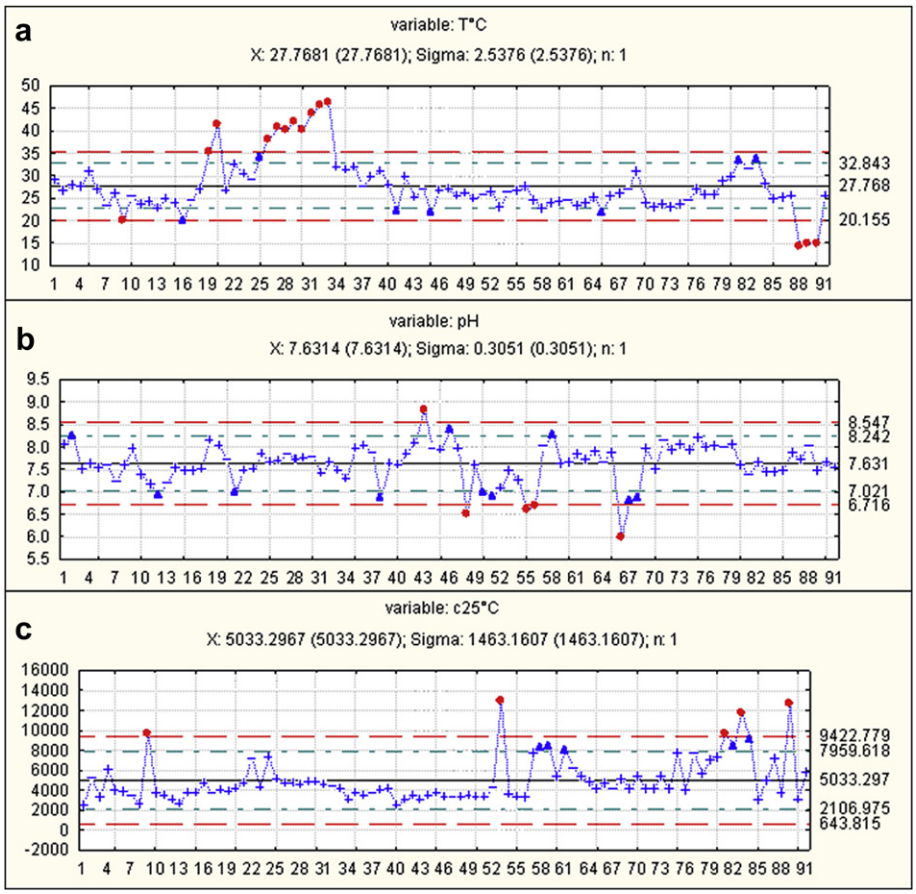

Fig. 4. Temperature (a), pH (b) and EC (c) variations of the current sampling.

in the region where the weathering of evaporites occurred. Therefore, factor 1 describes the salinization factor. The components of the salinization factor are similar to the 'Turonian groundwater salinization factor' in the western part of the study area (Abid, 2010) and to 'processes of the evaporate dissolution rocks' in Alto Guadalentín, SE Spain (Ceron et al., 2000) and in Bou-Areg, NE Morocco (Yaouti et al., 2009). The spatial distribution of the scores of factor 1 shows three areas with high values (Fig. 8a). The first area, located in the northern part of the plain, could be due to the influence of over-pumping, allowing the downward leakage of saline water from shallow aquifers. The second high score area, situated in the central part of the plain, could be related to the increase of water–rock interaction due to slow groundwater movement downstream in the Djeffara basin. The third area, in the southern part of the plain, could be related to the influence of marly-gypsum outcrops and to the processes of dissolution of the evaporite rocks (Quaternary and Triassic formation (Fig. 1) enriched in evaporate and gypsiferous materials). The low scores recorded around the Matamata region show the contribution of the Daher upland to the recharge of the aquifer system.

Axis II (15.36%) opposes Alkalinity, Mg^{2+} and K^{+} concentrations with temperature, pH and Ca^{2+} contents. This axis, basically representing the calco-carbonic parameters, describes factor dilution of groundwater by water recharge and/or mineralization by water–soil/rock interaction.

The opposite evolution of Ca^{2+} and Alkalinity (HCO_3^-) in factor 2 indicates that the increase of Ca^{2+} content in groundwater is essentially related to gypsum dissolution and cation exchange

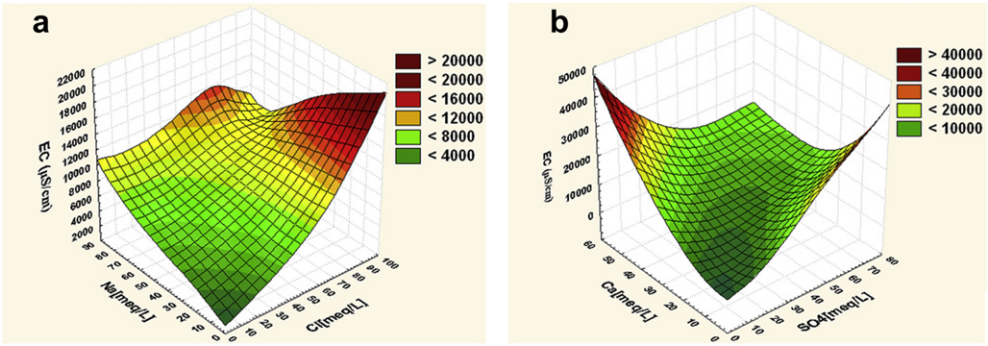

Fig. 5. 3D surface plot of EC (μS/cm) against Cl^- and Na^+ (a); and SO_4^{2-} and Ca^{2+} (b).

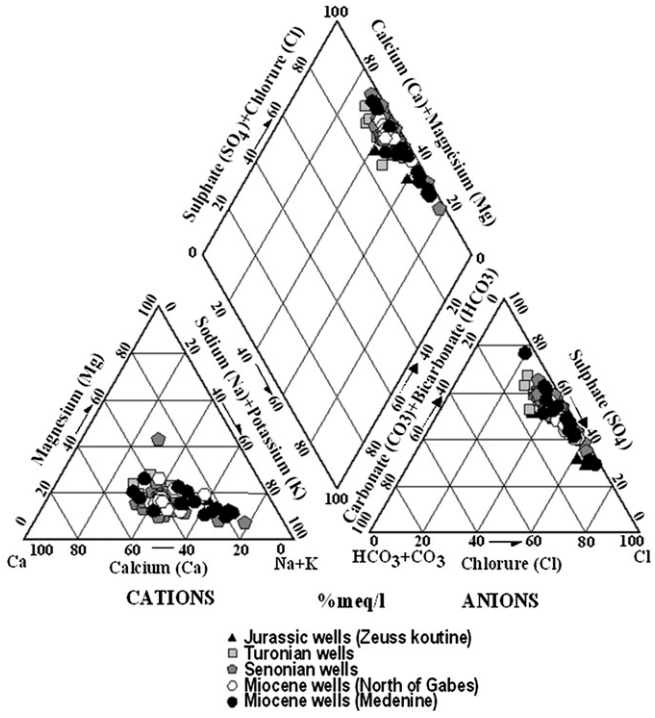

Fig. 6. Piper diagram of the current sampling.

processes, and not to carbonate weathering. The spatial distribution of factor 2 shows that high temperature and concentration of Ca^{2+} occur in the El Hamma region (Fig. 8b). This excess may be related to the upflow leakage of the deep Continental Intercalaire groundwater (SO_4^{2-}–Ca^{2+} water type) towards the Djeffara aquifer system via deep faults.

5.3. Hierarchical cluster analysis

The obtained diversity-based hierarchical dendrograms groundwater samples are depicted in Fig. 9. For this study, the Euclidean distance was chosen as the distance measure, or similarity measurement, between sampling sites. Cluster analysis allows the grouping of water samples according to their similarities in terms of physico-chemical characteristics and stable isotopes contents, as illustrated in the dendrogram (Fig. 9 and Table 5).

In this study, the phenon line was drawn across the dendrogram at a linkage distance of about 19 (Fig. 9). Thus, samples with a linkage distance lower than 19 are grouped into the same cluster. This position of the phenon line allows a division of the dendrogram into three main groups which can be further divided in 12 clusters of groundwater samples, named A1, A2, B1–B4, C1–C4, D1 and D2. As mentioned by Güler et al. (2002), the number of clusters could be defined by moving the position of the phenon line up or down on the dendrogram. Observation of the dendrogram reveals some indications of the level of similarity between the 12 clusters (Fig. 9). The first group is formed by clusters A1 and A2 and contains samples showing particularly high values of temperature and the most depleted stable isotopes contents. These samples, collected from the Senonian aquifer, present similar chemical facies (SO_4-mixed water type) and isotopic signature than Cl palaeogroundwater which strongly supports the hypothesis of the hydraulic communication between these two aquifers (Trabelsi et al., 2009). The second group is composed by clusters D1 and D2 and includes very similar samples located at the recharge zone (Daher upland) in the western part of the study area. This group corresponds to samples with low temperature and relatively enriched alkalinity and stable isotopes contents in relation with admixture with recent rainwater infiltration (see Table 1). The third group could be further divided in clusters B (B1–B4) and C (C1–C4), even if this subdivision takes place at a linkage distance of about 110. This group generally represents a middle course between the two previous groups showing transitional waters. This analysis therefore confirms the conclusions obtained in the hydrogeology and hydrochemistry studies.

6. Groundwater age distribution from isotopic data

6.1. Isotopes of water

Tritium is absent in the majority of the analyzed water samples, indicating the pre-bomb age of groundwater. Some traces of ^3H were found in well No.12 (1.3 TU) and No. 41 (2.8 TU). These ^3H contents are comparable with the current concentration of ^3H in local precipitation.

Nitrate is a chemical species that essentially originates from the land surface, and it is eventually removed from groundwater by denitrification with increased residence times (Chae et al., 2001). Therefore, it could be used to indicate the relative groundwater age. Table 1 shows that the nitrate levels are very low when $\delta^{18}O$ values are low, supporting the view that most groundwater was derived from palaeorecharge.

Stable isotopes ($\delta^{18}O$, δ^2H) have conservative properties and provide information on the groundwater recharge processes (Gat, 1971). The residence time of groundwater, in actively circulating

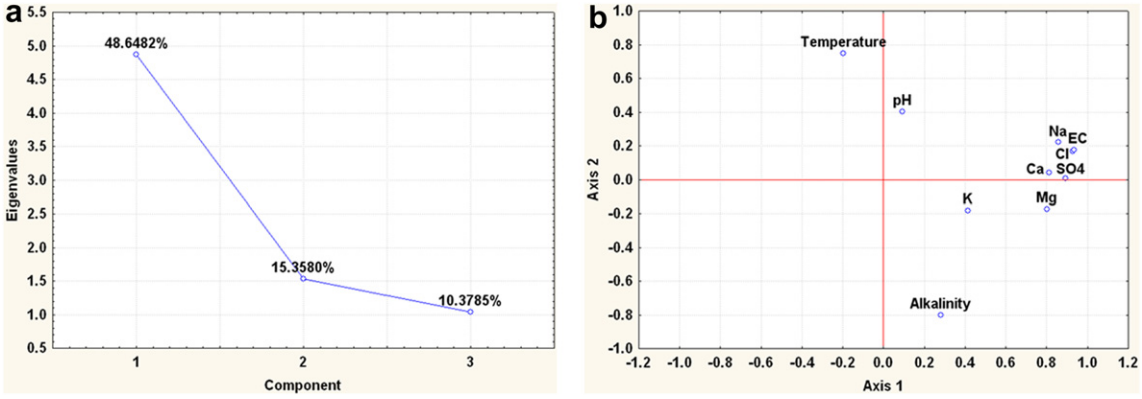

Fig. 7. Eigenvalues scree plot (a) and loading scatterplot (p1 vs. p2).

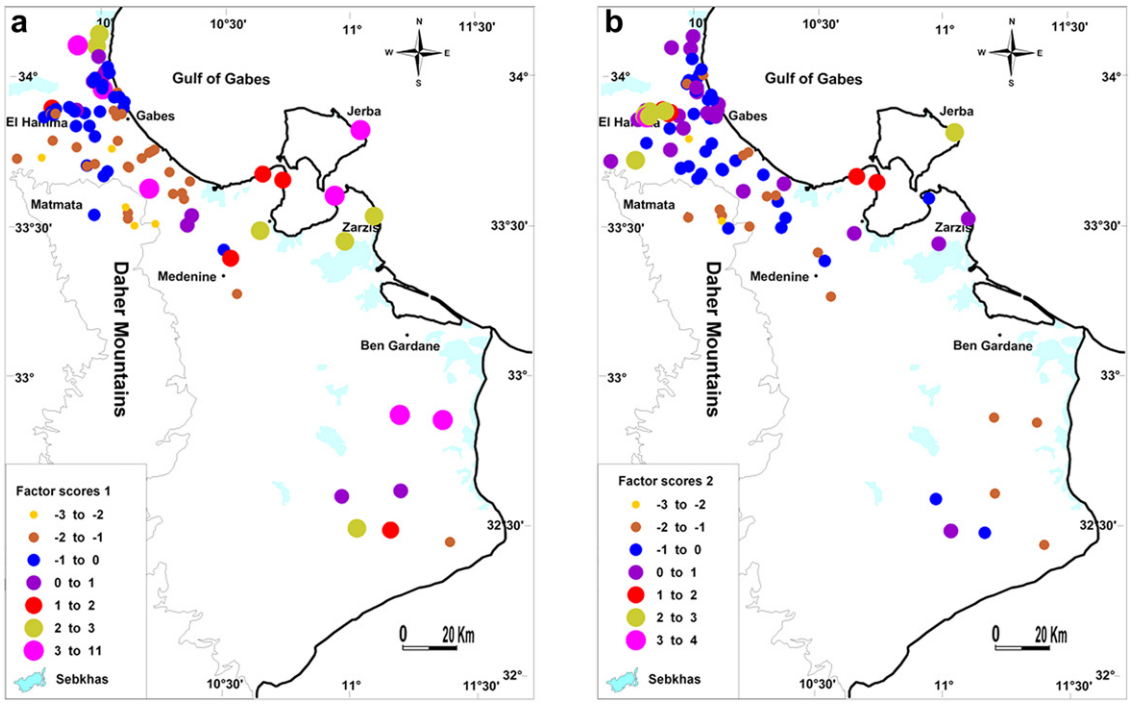

Fig. 8. Spatial distribution of F1 (a) and F2 (b) Factor scores for the current sampling.

systems, may range from tens to thousands of years. Therefore, changing climate should be recorded in palaeogroundwaters. A change in the stable isotope composition of groundwater indicating the transition from the Late Glacial to Holocene has been identified in many aquifers with waters of different ages. For instance, water, recharged in the Sahara, during the humid periods of the Quaternary, is systematically depleted in heavy isotopes as compared to modern precipitation, and has a d-excess lower than 10‰ (Rozanski, 1985; Rozanski et al., 1993; Gasse, 2002). Therefore, palaeogroundwaters from temperate and arid regions will be isotopically depleted with respect to modern waters and shifted along the Global Meteoric Water Line (GMWL) towards negative values.

The nearest relevant IAEA/WMO GNIP station is Sfax, for which there is a continuous temporal record of monthly means of $\delta^{18}O$ and $\delta^{2}H$ for rainfall covering the period 1992–2009 (IAEA/WMO, 2010). The weighted mean value of Sfax rain water is −4.4‰ vs. VSMOW for $\delta^{18}O$ and −24.9‰ vs. VSMOW for $\delta^{2}H$ (Abid, 2010). The $\delta^{18}O$ and $\delta^{2}H$ compositions of groundwater, for the current samples, range from −4.3‰ to −8.3‰ and from −30.4‰ to −65.9‰, respectively. In the $\delta^{2}H$ versus $\delta^{18}O$ diagram (Fig. 10, Table 1), most of the groundwater samples are situated below the GMWL defined by Craig (1961). A mixing line could be observed between two extreme values ([−4.3 $\delta^{18}O$‰, −30.4 $\delta^{2}H$‰]; [−8.3 $\delta^{18}O$‰, −63.4 $\delta^{2}H$‰]). The least depleted $\delta^{18}O$ and $\delta^{2}H$ values represent wells in the main recharge area in the west (No. 8). Within the stated analytical uncertainty (Table 1), their isotopic composition is close to the weighted mean values for modern rainfall in Sfax. However, some samples (e.g., wells No. 12 and No. 13) situated in elevated areas (Daher upland) are relatively depleted in both $\delta^{18}O$ and $\delta^{2}H$ comparing to the weighted mean values of modern rainfall. This depletion, which is about of −1.4‰ for $\delta^{18}O$ and about −6.9‰ for $\delta^{2}H$, is probably related to an altitude effect. The more impoverished waters are about −2.8 $\delta^{18}O$‰ and −27.5 $\delta^{2}H$‰ lighter than modern rainfall and must represent a cooler regime.

However, the most depleted $\delta^{18}O$ and $\delta^{2}H$ values (−8.28‰ and −65.85‰, for $\delta^{18}O$ and $\delta^{2}H$ respectively) are measured in the

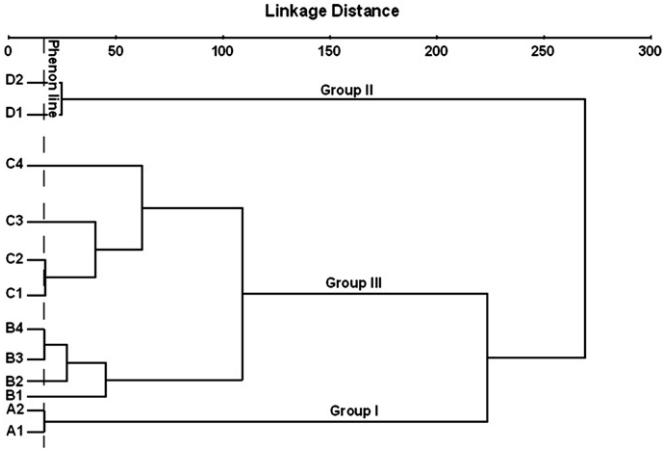

Fig. 9. Dendrogram based on agglomerative hierarchical clustering (Ward's method) for the 91 samples considered in this study.

Table 5
Samples contained in each of the clusters of the dendrogram shown in Fig. 9.

Group	Samples
A1	28, 30, 29, 27, 26, 25
A2	33, 32, 31, 20
B1	90, 89, 88
B2	83, 81, 80, 79, 84, 40
B3	91, 75, 58, 53
B4	61, 50, 51, 49, 48, 46, 47, 18, 56, 55, 6
C1	68, 66, 65, 64, 70, 59
C2	73, 62, 63, 60, 15, 37, 67, 21, 10
C3	52, 76, 54, 44, 71, 74, 57, 17, 14, 16, 43, 27, 7
C4	39, 34, 24, 23, 22, 82, 36, 19, 42, 69, 35, 38, 5
D1	87, 86, 85, 78, 77, 4, 2
D2	12, 45, 13, 11, 41, 9, 8, 3, 1

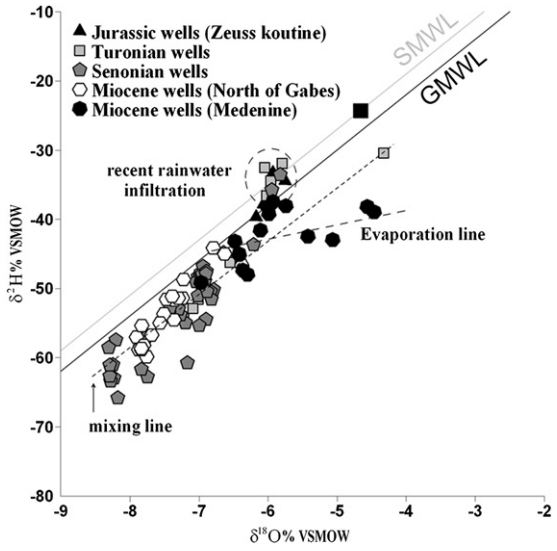

Fig. 10. $\delta^{18}O$ versus $\delta^{2}H$ for the current sampling. World meteoric water line (Craig, 1961) and Sfax meteoric water line have been plotted (IAEA/WMO, 2010), weighted mean isotopic content of Sfax precipitation is represented by a rectangle.

northwestern part of the basin in the El Hamma region. This isotopic composition could be explained by a mixing process with palaeogroundwaters of the CI aquifer (Abid et al., 2009; Trabelsi et al., 2009) by up leakage through the El Hamma Fault. This depleted isotope signature is characteristic of palaeowaters in the Western Sahara, partly explained by changes in rainfall amount and air humidity (Gasse, 2002). During the wet Holocene and Late Pleistocene, a decrease in stable isotope content of precipitation is suggested in contrast with modern patterns (Gasse, 2002). In addition, the measured content of nobles gases in the CI groundwater (Guendouz et al., 1997) confirm this climate change and indicates cooler recharge temperatures (ca. 5.5 °C) than present-day mean annual temperatures in the region (20.6 °C). This mixing with palaeogroundwater is supported by low ^{14}C activities and low NO_3^- concentrations measured in these groundwaters.

6.2. Carbonate system evolution and carbon isotopes

Radiocarbon data is required to confirm the hydrogeological model implied by isotopic data. However, this tracer which is serving as a dating tool of water in the arid zone has a specific set of research problems and numerous limitations in its interpretation. A major difficulty is assigning an appropriate correction scheme for ^{14}C dating (i.e., estimating the initial ^{14}C concentration at the time of recharge). One of the reasons for this is the variability of chemical and isotopic end-members, such as soil gas $\delta^{13}C$, ^{14}C and pCO_2, and carbonate mineral $\delta^{13}C$ and ^{14}C, used in the various ^{14}C correction schemes. For this reason, special attention must be paid to radiocarbon ages.

Radiocarbon activities and $\delta^{13}C$ values of DIC have been determined for 35 boreholes. It is apparent from Table 1 that ^{14}C activities and $\delta^{13}C$ values of DIC cover a wide range of values. The $\delta^{13}C$ content of the total DIC ranges from −4.7 to −13.5‰ vs. PDB for measured ^{14}C activities extending from 2 to 43 pmc. The highest measured radiocarbon content (43 pmc) was observed in relatively shallow well (No. 11) located in the Daher upland. In this well also tritium was perceived (ca. 1.3 TU) pointing to infiltration of fresh water. The lowest value (2 pmc) was found in wells No. 55 and No. 79 tapping the Senonian and the Miocene of Medenine aquifers located downstream in the basin.

The evolution of the C isotope composition of the DIC pool of the infiltrating water recharging the Djeffara groundwater system can be addressed using the open- and closed system conditions with respect to dissolution of carbonate phases in the unsaturated zone (e.g., Deines et al., 1974; Clark and Fritz, 1997). These two simple models provide a general conceptual framework in which the C isotope data could be linked to the size of the DIC pool.

The ^{14}C activities and $\delta^{13}C$ values measured in the sampled boreholes were plotted as a function of the size of the DIC reservoir (Fig. 11a and b). Superimposed are different trend lines predicted by the simple models mentioned above. The trajectories marked in Fig. 11 by solid lines (black and grey) indicate the initial evolution of the C isotope composition of the DIC pool. First, soil CO_2 of prescribed characteristics (partial pressure 0.01 atm, ^{14}C activity equal to 100 pmc, $\delta^{13}C$ equal to −20‰) dissolves gradually in the infiltrating water until saturation with respect to $CaCO_3$ (^{14}C activity equal to 0 pmc, $\delta^{13}C$ value equal to 0‰) is reached. The saturation points are marked by stars. From those points, the solution was allowed to evolve further under closed-system conditions (dashed lines grey and black) by adding new C in the form of CO_2, devoid of ^{14}C. Thus, two different $\delta^{13}C$ values of this additional C were considered: −20‰ and −5‰ vs. PDB. The first value corresponds to CO_2 derived from decomposition of sedimentary organic C, the second one represents the deep mantle CO_2.

As seen in Fig. 11a, the ^{14}C data cluster around the closed-system trend lines with two-step addition of C to the solution. Some data

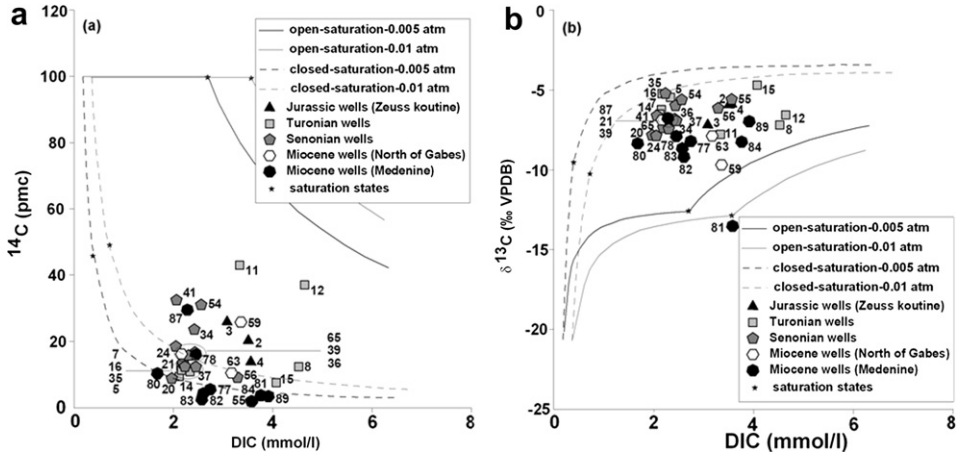

Fig. 11. Carbon isotope evolution of the DIC reservoir under open- and closed system conditions. Stars indicate saturation of the solution with respect to $CaCO_3$. Subsequent evolution of the DIC reservoir (grey lines), resulting from input of additional C, was calculated via consecutive equilibrium stages with a solid carbonate phase (see text for details).

points are located either above or below the trend lines. The location of data points in Fig. 11a above the trend lines, revealing higher ^{14}C activities than the modeled ones for the closed-system model, suggests that in reality the conditions in recharge area(s) are somewhere between open- and closed-system conditions with respect to soil CO_2, although the position of data points below the trend line (Fig. 11a) could be interpreted in terms of water age. The distance between the trend line and the given data point (between ca. 1 and 6 pmc) could be then converted to a radiocarbon age. The resulting ages would be in the order of 1–9 ka.

While the ^{14}C activity falls on the line representing the closed-system model, its $\delta^{13}C$ value indicates mixed-system (between open- and closed-system conditions). The $\delta^{13}C$ data (Fig. 11b) provide an additional constraint on the process of adding additional C to the system. In this diagram, it is clear that the calculated DIC contents assuming closed-system model are substantially lower than the measured values. In contrast, under open-system conditions, the calculated DIC content is in the range of measured values. The admixture of CO2 of mantle origin leads to chemical and isotope characteristics of DIC pool which are in broad agreement with the measured values.

An attempt was made to estimate groundwater residence time using correction models (Trabelsi, 2009; Zouari et al., 2010) in Djeffara aquifer system. The calculated ages indicate different recharge periods mostly occurring during the Holocene and Pleistocene wet periods:

- Present day to the Lower Holocene (<10 000 BP) with $\delta^{18}O$ ranging between −6.05 and −4.3‰ vs VSMOW as for modern rainwater. This recent recharge is located in Daher upland and near to Medenine Fault in the western part of the basin;
- The last deglaciation period of 10 000–18 000 BP, observed for some water samples of the Miocene aquifer. These groundwater are more depleted in $\delta^{18}O$ (−6.9 and −6.3‰ vs SMOW) which is in agreement with cooler climate conditions of this period;
- Late Pleistocene (>20 000 BP) for the Senonian groundwater with similar depleted $\delta^{18}O$ contents (−6.9 and −6.2‰ vs VSMOW). This groundwater age confirms the upward leakage from CI plaeogroundwater (Abid et al., 2009).

7. Conclusions

Statistical and geochemical analyses were applied to the hydrochemical data set and to provide insight into the regional factors and processes controlling the chemical composition and degree of salinity of groundwater in the study area.

The results of the factor analysis showed 2 factors (F1 and F2), that explained 64% of the total variance in the groundwater quality. Factor F1 (described as the salinization factor) included EC, Cl^-, Na^+, Ca^{2+}, Mg^{2+}, SO_4^{2-} and Cl^-, and factor F2 (the dilution processes) included Alkalinity, Mg^{2+} and K^+ in opposition to temperature, pH and Ca^{2+}. The spatial distribution of the factor scores at individual wells delineated boundaries that define the areas of high salinization. Areas of high scores of factor 1 close to the northern part of the plain are due to the influence of overpumping, and, at the central part of the plain, the salinization is linked to the influence of increased time of water–rock interaction. At the southern part of the plain, the salinization could be related to the influence of marly-gypsum outcrops. High scores of factor 2 are located in the Daher upland, where the recharge from the Upper Cretaceous carbonates of Matmata regions refreshes the groundwater and enriches the area in HCO_3^-.

Environmental isotopes were used to characterize chemistry and groundwater dynamics flow at the Djeffara aquifer system in the eastern part of Southern Tunisia. The modelling of isotopic evolution of the DIC pool yielded some information of the presence of additional source of carbon with the isotope characteristics typical for mantle CO_2 ($\delta^{13}C \approx -5‰$) which can explain the range of $^{13}C/^{12}C$ and $^{14}C/^{12}C$ ratios observed in DIC pool of the analyzed groundwater samples. Stable isotope composition of groundwater samples representing Djeffara and CI aquifers provide strong evidence for large scale interaction between both systems. It is apparent from the presented data that upflow leakage from the CI aquifer, favored by deep faults, constitutes an important recharge mechanism for the Djeffara aquifer. The presence of ^3H in some wells points to the contribution of recent infiltration occurring after the 1950s.

Acknowledgments

This study was carried out within the framework of the regional IAEA project RAF/8/035.

References

Abid, K., 2010. Identification et caractérisation hydrogéologique et géochimique de la nappe du Continental Turonien dans le Sud tunisien et sa relation avec les aquifères adjacents. Thèse de Doctorat, Ecole Nationale d'Ingénieurs de Sfax, Tunisie, 191pp.

Abid, K., Trabelsi, R., Zouari, K., Abidi, B., 2009. Caractérisation hydrogéochimique de la nappe du continental intercalaire (Sud tunisien). Hydrological Sciences Journal des Sciences Hydrologiques 54, 526–537.

Ben Baccar, B., 1982. Contribution à l'étude hydrogéologique de l'aquifère multicouche de Gabès Sud. PhD thesis, Paris-Sud (Orsay), 115pp.

Benton, M.J., Bouaziz, S., Buffetaut, E., Martill, D., Ouaja, M., Soussi, M., Trueman, C., 2000. Dinosaurs and other fossil vertebrates from fluvial deposits in the lower Cretaceous of Southern Tunisia. Palaeolgeography Palaeoclimatology Palaeoecology 157, 227–246.

Bouaziz, S., 1995. Etude de la tectonique cassante dans la plate-forme et l'Atlas Sahariens (TunisieMéridionale): Evolution des paléochamps de contraintes et implications géodynamiques. PhD thesis, Fac. Sc. De Tunis, 301pp.

Bouaziz, S., Barrier, E., Soussi, M., Turki, M.M., Zouari, H., 2002. Tectonic evolution of the northern African margin in Tunisia from paleostress data and sedimentary record. Tectonophysics 357, 227–253.

Castany, G., 1954. L'accident Sud tunisien, son âge et ses relations avec l'accident Sud atlasique d'Algérie. Note H. Devaux, Bull. Soc. Franç. Phys, 219 (1925) p 90, séance du 8 Février 1954.

Ceron, J.C., Jimenez-Espinosa, R., Pulido-Bosch, A., 2000. Numerical analysis of hydrogeochemical data: a case study (Alto Guadalentõan, southeast Spain). Applied Geochemistry 15, 1053–1067.

Chae, G.T., Yun, S.T., Kim, S.R., Hahn, C., 2001. Hydrogeochemistry of seepage water collected within the Youngcheon Diversion Tunnel, Korea: source and evolution of SO4-rich groundwater in sedimentary terrain. Hydrological Processes 15, 1565–1583.

Clark, I.D., Fritz, P., 1997. Environmental Isotopes in Hydrology. Lewis Publishers, Boca Raton, USA.

Colpen, T.B., Wildman, J., Chen, J., 1991. Improvement in the gaseous hydrogen-water equilibration technique for hydrogen isotopes ration analysis. Analytical Chemistry 63, 910–912.

Cook, P., Herczeg, A.L., 2000. Environmental Tracers in Subsurface Hydrology. Kluwer Academic Publishers, NewYork.

Craig, H., 1961. Isotopic variations in meteoric waters. Science 133, 1702–1703.

Deines, P., Harmon, R.S., Langmuir, D., 1974. Stable carbon isotope ratios and the existence of a gas phase in the evolution of carbonate ground waters. Geochimica et Cosmochimica Acta 38, 1147–1164.

Epstein, S., Mayeda, T.K., 1953. Variations of 18O content of waters from naturel sources. Geochimica et Cosmochimica Acta 4, 213–224.

Etcheverry, D., 2002. Valorisation des Méthodes Isotopiques pour les Questions Pratiques Liées aux eaux Souterraines. Office Fédéral des Eaux et de la Géologie, Lausanne.

Fontes, J.Ch, 1971. Un ensemble destiné à la mesure de l'activité du radiocarbone naturel par scintillation liquide. Revue Geographie Physique et Géologie Dynamique 13 (1), 67–86.

Fontes, J.Ch, 1980. Environmental isotopes in groundwater hydrology. In: Fritz, P., Fontes, JCh (Eds.), Handbook of Environmental Isotope Geochemistry. Elseiver, Amsterdam, pp. 75–140.

Gabtni, H., Jallouli, C., Mickus, K.L., Zouari, H., Turki, M.M., 2009. Deep structure and crustal configuration of the Jeffara basin (Southern Tunisia) based on regional gravity, seismic reflection and borehole data: How to explain a gravity maximum within a large sedimentary basin? Journal of Geodynamics 47, 142–152.

Gasse, F., 2002. Diatom-inferred salinity and carbonate oxygen isotopes in Holocene waterbodies of the Western Sahara and Sahel (Africa). Quaternary Science Reviews 21, 737–767.

Gat, J.R., 1971. Comments on the stable isotope method in the regional groundwater investigation. Water Resources Research 7, 980–993.
Gonfiantini, R., Conrad, G., Fontes, J.Ch., Sauzy, G., Payne, B.R., 1974. Etude isotopique de la nappe du Continental Intercalaire et ses relations avec les autres nappes du Sahara Septentrional, IAEASM- 182/25. In: Isotope Techniques in Groundwater Hydrology, vol. I. IAEA, Vienna, pp. 227–241.
Guendouz, A., Moulla, A., Edmunds, W.M., Shand, P., Poole, J., Zouari, K., Mamou, A., 1997. Paleoclimatic information contained in groundwaters of the Grand Erg Oriental, N. Africa. Isotope Techniques in the Study of Past and Current Environmental Changes in the Hydrosphere and Atmosphere. IAEA, Vienne. 555–571.
Güler, C., Thyne, G.D., McCray, J.E., Turner, A.K., 2002. Evaluation of graphical and multivariate statistical methods for classification of water chemistry data. Hydrogeology Journal 10, 455–474.
IAEA/WMO, 2010. Global network of isotopes in precipitation. The GNIP database. http://isohis.iaea.org.
Jackson, J.E., 1991. A User's Guide to Principal Components. Wiley, New York.
Kallel, R., 2003. Hydrologie de la Jeffara tunisienne. Rapport interne. CRDA de Gabes.
Mamou, A., 1990. Caractéristiques, evaluation, gestion des ressources en eau du Sud Tunisien. PhD thesis, University of Paris South, Paris.
Meglen, R.R., 1992. Examining large databases: a chemometric approach using principal component analysis. Marine Chemistry 39, 217–237.
Mellinger, M., 1987. Multivariate data analysis: its methods. Chemometrics and Intelligent Laboratory Systems 2, 29–36.
Rozanski, K., 1985. Deuterium and oxygen-18 in European groundwaters—links to atmospheric circulation in the past. Chemical Geology (Isotope Geoscience Section) 52, 349–363.
Rozanski, K., Araguàs-Araguàs, L., Gonfiantini, R., 1993. Isotopic patterns in modern global precipitation. In: Swart, P.K., Lohmann, K.C., McKenzie, J., Savin, S. (Eds.), Climate Change in Continental Isotopic Records. Geophysical Monograph Series, vol. 78. AGU, Washington, DC, pp. 1–36.
StatSoft, Inc., 1995. STATISTICA for Windows [Computer program manual]. Tulsa, OK.
Taylor, C.B., 1977. Tritium enrichment of environmental waters by electrolysis: development of cathodes exhibiting high isotopic separation and precise measurements and applications. High Tatras, Czechoslovakia, October 1975, Bratislava.
Taylor, R.E., 1987. Radiocarbon Dating. An Archaeological Perspective. Academic Press, Orlando.
Trabelsi, R., 2009. Caractérisation Hydrogéologique et Geochimique du systeme aquifere de la Djeffara (sud-est tunisien): Modélisation et Intrusion marine. PhD Thesis National School of Engineers of Sfax Tunisia, 219pp.
Trabelsi, R., Kacem, A., Zouari, K., Rozanski, K., 2009. Quantifying regional groundwater flow between continental Intercalaire and Djeffara aquifers in southern Tunisia using isotope methods. Environmental Geology 58, 171–183.
Vega, M., Pardo, R., Barrado, E., Deban, L., 1998. Assessment of seasonal and polluting effects on the quality of river water by exploratory data analysis. Water Research 32, 3581–3592.
Wenning, R.J., Erickson, G.A., 1994. Interpretation and analysis of complex environmental data using chemometric methods. Trends in Analytical Chemistry 13, 446–457.
Willet, P., 1987. Similarity and Clustering in Chemical Information Systems. Research Studies Press, Wiley, NY.
Yaouti, F.E.l., Mandour, A.E.l., Khattach, D., Benavente, J., Kaufmann, O., 2009. Salinization processes in the unconfined aquifer of Bou-Areg (NE Morocco): a geostatistical, geochemical, and tomographic study. Appied Geochemistry 24, 16–31.
Zouari, K., Trabelsi, R., Chkir, N., 2010. Using geochemical indicators to investigate groundwater mixing and residence time in the aquifer system of Djeffara of Medenine (Southeastern Tunisia). Hydrogeology Journal 19, 209–219.